Biomaterials 62 (2015) 155–163

Contents lists available at ScienceDirect

Biomaterials

journal homepage: www.elsevier.com/locate/biomaterials

Biomimetic DNA nanoballs for oligonucleotide delivery

Mi-Gyeong Kim [a, 1], Joo Yeon Park [a, 1], Gayong Shim [a], Han-Gon Choi [b], Yu-Kyoung Oh [a, *]

[a] College of Pharmacy and Research Institute of Pharmaceutical Sciences, Seoul National University, Seoul 151-742, Republic of Korea
[b] College of Pharmacy, Hanyang University, Ansan, Republic of Korea

ARTICLE INFO

Article history:
Received 20 January 2015
Received in revised form
15 April 2015
Accepted 21 April 2015
Available online 5 June 2015

Keywords:
DNA nanoballs
Rolling circle amplification
Biomimetic condensation
Antisense oligonucleotides
Sequence-specific loading

ABSTRACT

Here, we designed biomimetic DNA nanoballs for delivery of multiple antisense oligonucleotides (ASOs). DNA templates with ASOs-complementary sequences were amplified by rolling circle amplification (RCA). RCA products were loaded with two types of ASOs by hybridization, condensed using adenovirus-derived Mu peptide, and coated with hyaluronic acid (HA) for delivery into CD44-overexpressing tumor cells. HA-coated, Mu peptide-condensed, dual ASO-loaded DNA nanoballs (HMA nanoballs) showed considerable cellular entry of Cy5-incorporated RCA product DNA and fluorescent ASOs, whereas Mu peptide-condensed, dual ASO-loaded DNA nanoballs (MA nanoballs) revealed limited uptake. Dual ASOs, Dz13 and OGX-427, delivered by HMA nanoballs could reduce the levels of protein targets and exert anticancer effects. Enhanced tumor distribution was observed for fluorescent HMA nanoballs than the corresponding MA nanoballs. Upon intravenous co-administration with doxorubicin, HMA nanoballs exerted the greatest anti-tumor effects among the groups. These results suggest HMA nanoballs as a nanoplatform for sequence-specific delivery of multiple ASOs and other functional oligonucleotides.

1. Introduction

Recently, functional oligonucleotides have been studied as a major class of nucleic acid-based therapeutics [1]. Antisense oligonucleotides (ASOs) and micro RNA are examples of oligonucleotides with therapeutic potentials. However, these oligonucleotides suffer from drawbacks, such as instability against nucleases and limited cellular uptake owing to their high negative charges. To overcome these drawbacks, researchers delivered oligonucleotides using cationic lipid or polymer-based delivery systems. Cationic nanoparticles have previously been used to deliver single-stranded oligonucleotides based on charge–charge loading to cationic liposomes [2,3] and polymer-based nanoparticles [4,5]. However, the cationic nanoparticle-associated cytotoxicity [6] requires the development of other carriers not cationic as well as biomimetic for delivery of oligonucleotides.

Rolling circle amplification (RCA) is an enzymatic process that produces a single-stranded DNA (ssDNA) from a circular template. The resulting ssDNA is composed of complementary-sequence repeats of the circular template. RCA technology was originally used for DNA detection in genomics; however, additional applications using RCA have since been reported [7]. Recently, RCA was applied to construct DNA nanostructures and DNA hydrogels [8–11].

In this study, we used RCA-amplified DNA to produce an oligonucleotide delivery system. As model oligonucleotides, we chose two ASO oligonucleotides. To load ASO to the delivery system, we used sequence-specific hybridization rather than cationic nanoparticle-based charge–charge interaction. The template for RCA was designed to have complementary sequences for two different ASOs and to produce poly-binding sites for ASOs upon RCA amplification. Exploiting the DNA condensation mechanisms of viruses, we employed cationic Mu peptides derived from the adenovirus core complex to condense ASO-hybridized RCA products (ARP) and produce DNA nanoballs. The surface of ASO-loaded DNA nanoballs was coated with hyaluronic acid (HA), a ligand for CD44 receptors overexpressed by tumor cells [12], for tumor-targeted delivery.

Here, we demonstrated that DNA nanoballs with ASO-complementary sequences could provide sequence-specific loading of dual ASOs, and coating with HA promoted CD44 receptor-mediated delivery of ASOs to tumor cells. Importantly, ASOs delivered by HA-coated DNA nanoballs silenced the expression of their target mRNAs of ASO, exerting potent anticancer effects in vitro and in vivo.

* Corresponding author.
E-mail address: ohyk@snu.ac.kr (Y.-K. Oh).
[1] Both authors contributed equally to this work.

http://dx.doi.org/10.1016/j.biomaterials.2015.04.037
0142-9612/

2. Materials and methods

2.1. Construction of ASO-hybridized DNA nanoballs

ASO-hybridized DNA nanoballs were constructed by (1) amplifying ssDNA containing ASO-binding sites by RCA, (2) hybridizing with ASO, and (3) condensing with cationic Mu peptides. In the first step, an RCA template for complementary binding with ASOs was circularized using primers. Briefly, 0.5 μM of 5′-phosphorylated linear ssDNA template and primer (Macrogen Inc., Daejeon, Republic of Korea) were annealed in hybridization buffer (10 mM Tris–HCl, 1 mM EDTA, 100 mM NaCl, pH 8.0) and mixed with T4 DNA ligase (125 units/mL) (Thermo Scientific, Waltham, MA, USA) to close the nick in the circular RCA template. After inactivating T4 DNA ligase by heating to 70 °C, the circular RCA template (200 μL) was incubated at 30 °C for 12 h with phi29 DNA polymerase (100 units/mL) (Thermo Scientific) and 2 mM dNTPs (Intron Biotechnology Inc., Seoul, Republic of Korea). In some experiments, fluorescent RCA products were prepared by adding 25 μM of Cy5-dCTP to 2 mM dNTPs during the RCA reaction. After heat-inactivating phi29 DNA polymerase at 70 °C for 10 min, residual dNTPs were removed by centrifugation at 13,000 rpm for 10 min. The resulting pellet of RCA product was resuspended in water, and its concentration was measured using a Nanodrop spectrophotometer (Thermo Scientific). Two different ASOs—Dz-13 (125 μg) and OGX-427 (125 μg)—were hybridized with 1 mL of RCA products (500 μg DNA/mL) by heating at 95 °C for 10 min and then cooling gradually at room temperature. The cationic Mu peptide (Peptron, Daejeon, Republic of Korea) was added to the resulting dual ARP at a weight ratio of 1:1 to form a nanoball-like structure. The resulting complexes of Mu-condensed, dual ASO-hybridized DNA nanoballs (MA nanoballs) were mixed with 214 kDa HA (Lifecore Biomedical Inc., Chaska, MN, USA) at a DNA:Mu:HA weight ratio of 1:1:5. HA-coated, Mu-condensed, dual ASO-hybridized DNA nanoballs (HMA nanoballs) were stored at 4 °C until use. In some experiments, RCA products alone were mixed with Mu peptide at a weight ratio of 1:1, and coated with HA at a DNA:Mu:HA ratio of 1:1:5 to produce HA-coated, Mu-condensed DNA nanoballs without ASOs (HM nanoballs).

2.2. Quantification of hybridized ASOs

The two ASOs, Dz-13 and OGX-427, were labeled using different fluorescent dyes to measure the efficiency of hybridization to RCA products. Fluorescein (FAM)-conjugated Dz-13 and 6-carboxy-x-rhodamine (ROX)-tagged OGX-427 were supplied by Bioneer Corporation (Daejeon, Republic of Korea). The fluorescent dye-modified ASOs, FAM-Dz-13 and ROX-OGX-427 (5.5 μg each), were hybridized with 100 μL of RCA products (200 μg DNA/mL). The procedure described in section 2.1 was adapted for loading fluorescent dye-modified ASOs to RCA products. Unloaded fluorescent ASOs were removed by repeated centrifugation at 13,000 rpm for 10 min, and the fluorescence intensity of the supernatants was measured using a Spectramax Gemini XS microplate fluorometer (Molecular Devices Cooperation, Sunnyvale, CA, USA). The amounts of hybridized Dz-13 and OGX-427 were calculated from calibration curves of fluorescence intensity of each fluorescent dye-labeled ASO as a function of concentration.

2.3. Characterization study of DNA nanoballs

The sizes of various DNA nanoballs, with or without Mu peptide-induced condensation and HA coating, were measured by dynamic light scattering. The zeta potentials of DNA nanoballs were also measured by laser Doppler microelectrophoresis at an angle of 22° using an ELSZ-1000 instrument (Photal, Osaka, Japan). The morphology of DNA nanoballs was visualized by scanning electron microscopy (SEM) using a Supra 55VP system (Carl Zeiss, Oberkochen, Germany). The stability of ARP, MA nanoballs, and HMA nanoballs against nucleases was tested by incubating 1 μg of DNA with 1 unit of DNase I (Sigma, St. Louis, MO, USA) at 37 °C for 30 min. The mixture was electrophoresed on 1% agarose gels and visualized by staining with Safe-Pinky dye (GenDepot, Barker, TX, USA).

2.4. Cellular uptake test of DNA nanoballs

Cellular uptake of various DNA nanoballs was evaluated by preparing fluorescent DNA nanoballs using 25 μM Cy5-dCTP (Perkin Elmer, Boston, MA, USA) and DNA nanoballs carrying fluorescent dye-modified ASOs, as described above. KB human epidermal carcinoma cells (American Type Culture Collection, Rockville, MD, USA) were cultured in RPMI-1640 medium (Welgene, Daegu, Korea) supplemented with 10% fetal bovine serum and 100 units/mL penicillin plus 100 μg/mL streptomycin. KB cells were seeded onto poly-L-lysine coated coverslips (BD Biosciences, San Jose, CA, USA) in 24-well plates (SPL Life Sciences, Pocheon, Republic of Korea) at a density of 8×10^4 cells/well. The next day, cells were treated with Cy5-dCTP–incorporated fluorescent DNA nanoballs or fluorescent dye-modified ASO-loaded DNA nanoballs at a concentration of 20 μg DNA/well. In some experiments, cells were pre-incubated with 10 μM HA for 2 h prior to treatment with DNA nanoballs. For fluorescence microscopy, cells were washed and fixed with 4% paraformaldehyde in phosphate-buffered saline (PBS) for 15 min, and stained with 4′,6-diamidino-2-phenylindole dihydrochloride (DAPI). The fluorescence of cells was observed using a confocal laser-scanning microscope (LSM 5 Exciter; Carl Zeiss, Inc., Jena, Germany). For flow cytometry, the cells were harvested and washed three times with cold PBS containing 2% fetal bovine serum, and analyzed using a BD FACSCalibur system equipped with Cell Quest Pro software (BD Biosciences).

2.5. Knockdown study of target protein expression

In vitro silencing of target protein expression by DNA nanoballs was evaluated by Western blotting. Various DNA nanoballs were applied to KB cells seeded in 6-well plates. After a 1-h incubation, the cell medium was replaced and cells were incubated for an additional 24 h. Whole-cell lysates were then prepared, and extracted proteins were quantified using a BCA protein assay kit (Thermo Scientific) according to the manufacturer's instruction. Proteins in samples were separated by sodium dodecyl sulfate-polyacrylamide gel electrophoresis (SDS-PAGE) on 10% gels and then transferred onto polyvinylidene difluoride membranes (Hybond-ECL; Amersham Biosciences, Piscataway, NJ, USA). Membranes were probed by Western blotting using specific antibodies to c-Jun (1:500, sc-1694; Santa Cruz Biotechnology, CA, USA), Hsp27 (1:500, sc-9012; Santa Cruz Biotechnology), and glyceraldehyde-3-phosphate dehydrogenase (GAPDH; 1:1000, sc25778; Santa Cruz Biotechnology).

2.6. Assessment of DNA nanoball anticancer activity

The cancer cell-killing effect of various DNA nanoballs was quantitatively evaluated using a Cell Counting Kit 8 (CCK-8; Dojindo Laboratories, Kumamoto, Japan) and visualized by staining of live cells after treatment with DNA nanoballs. KB cells were seeded in 48-well plates at a density of 6×10^4 cells/well. The next day, the cells were treated with various types of DNA nanoballs at a constant

amount of DNA (20 μg/well). After a 1-h incubation in the presence or absence of 1 μM doxorubicin (Dox), the cell medium was replaced and cells were incubated for an additional 24 h. Cell viability was then measured by CCK-8 assay. For CCK-8 assays, 20 μL of CCK-8 solution was added to each well and plates were incubated for 30 min. The absorbance of the medium at 450 nm was then measured colorimetrically using an enzyme-linked immunosorbent assay (ELISA) reader (Sunrise-Basic TECAN, Mannedorf, Switzerland). For live cell staining, cells were stained with calcein-AM (Molecular Probes, Eugene, OR, USA) after treatment with various DNA nanoballs.

2.7. In vivo molecular imaging

The in vivo tumor distribution of Cy5-dCTP–labeled DNA nanoballs was assessed by molecular imaging. Five-week-old athymic nude mice (Orient Bio Inc., Seongnam, Korea) were subcutaneously inoculated with 5×10^5 kB cells. After tumors had reached a volume of ~100 mm^3, fluorescent HMA or MA nanoballs were intravenously injected into the mice at a dose of 4 mg DNA/kg. After 1 h, the intensity of Cy5 signals was monitored using an eXplore Optix system (Advanced Research Technologies Inc., Montreal, Canada) and scanned using a 670 nm laser at a power of 25 mW and a count time of 0.3 s/point.

2.8. In vivo study of anti-tumor effects

The in vivo anti-tumor activity of DNA nanoballs was evaluated by measuring tumor growth-inhibitory effects. KB cells (5×10^5 cells) were subcutaneously inoculated into the dorsal right side of 5-wk-old athymic nude mice (Orient Bio). After tumors had become established, DNA nanoballs and Dox were intravenously administrated at a DNA dose of 8 mg/kg and a Dox dose of 3 mg/kg. For MA and HMA nanoballs, the doses of ASOs were 2 mg/kg each for Dz-13 and OGX-427. Mice were treated with the mixture of DNA nanoballs and Dox every other day for a total of three injections. Tumor size was measured in two dimensions using a slide caliper every 2 days, and tumor volume was calculated as $a \times b \times b \times 0.5$, where a and b are the lengths of the largest and smallest dimensions. The mice were sacrificed on day 21, and tumor tissues were extracted and weighed.

2.9. Statistics

All statistical analyses were performed using analysis of variance (ANOVA) with a post hoc Student–Newman–Keuls test. SigmaStat software (version 3.5; Systat Software, Richmond, CA, USA) was used for the analyses, and a p-value less than 0.05 was considered statistically significant.

3. Results

3.1. Sequence-specific hybridization of dual ASOs onto DNA nanoballs

The sequences of scrambled and dual ASO-complementary RCA templates are illustrated in Fig. 1A and B, respectively. ARP was formed by hybridization of Dz13 and OGX-427 (Fig. 1C). Loading amounts of Dz13 and OGX-427 onto RCA products depended on the sequences of RCA templates. As compared to RCA products of scrambled template, the RCA products of dual ASO-complementary RCA templates provided 8.1- and 6.7-fold higher loading amounts for Dz13 and OGX-427, respectively (Fig. 1D). ARP was then treated with adenovirus-derived Mu peptide to produce Mu peptide-

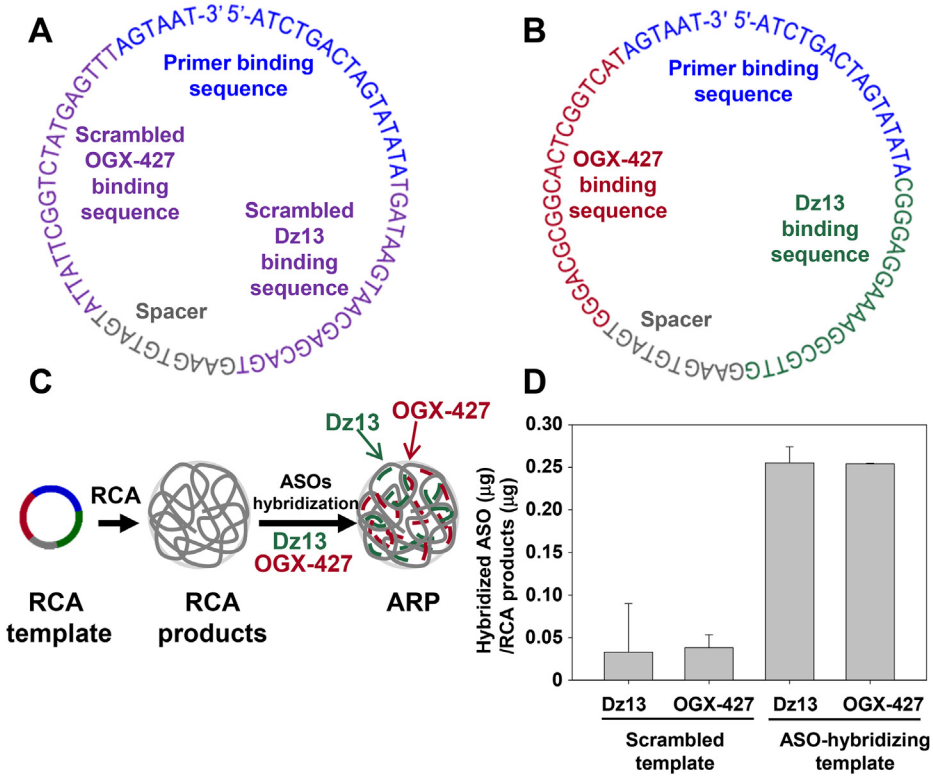

Fig. 1. RCA template and hybridization efficiency. (A) Secondary structure of scrambled RCA template. (B) Secondary structure of a dual ASO-hybridizing RCA template for Dz-13 and OGX-427. (C) RCA products with poly ASO-binding sequences were hybridized with two ASOs, Dz-13 and OGX-427, to produce dual ARP. (D) The hybridization efficiencies of the ASOs, Dz-13 and OGX-427, were tested for products of scrambled RCA templates and dual ASO-hybridizing RCA templates using fluorescently labeled ASOs (FITC-Dz-13, ROX-OGX-427).

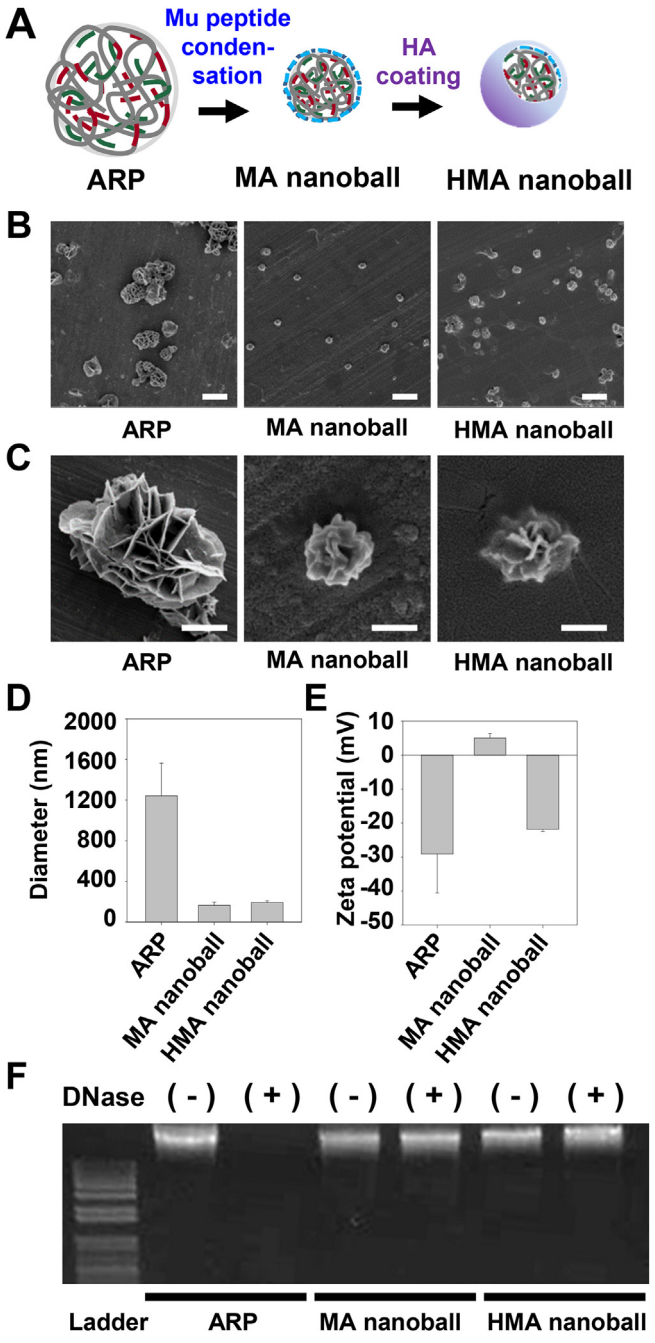

Fig. 2. Schematic illustration and morphology of DNA nanoballs. (A) Illustration of the HMA nanoball preparation scheme. Dual ARP were mixed with adenovirus core complex-derived Mu peptide to form MA nanoballs. The surfaces of MA nanoballs were coated with HA to produce HMA nanoballs. (B,C) The morphologies of ARP, MA nanoballs, and HMA nanoballs were observed by SEM at different magnifications. Scale bar: 2 μm for all groups (B). Scale bar: 800 nm for ARP and 200 nm for MA nanoball and HMA nanoball (C). (D) The sizes of ARP, MA nanoballs, and HMA nanoballs were measured by dynamic light scattering. (E) Zeta potential values of ARP, MA nanoballs, and HMA nanoballs were determined by laser Doppler microelectrophoresis. (F) The stability of ARP, MA nanoballs, and HMA nanoballs against DNase I was tested by incubation with 1 unit of DNase I for 30 min, followed by electrophoresis on a 1% agarose gel.

condensed, dual ASO-loaded DNA nanoballs (MA nanoballs). HA was then complexed with MA nanoballs to form HA-coated, Mu peptide-condensed, dual ASO-loaded DNA nanoballs (HMA nanoballs) for targeted delivery of ASOs to tumors overexpressing the receptor, CD44.

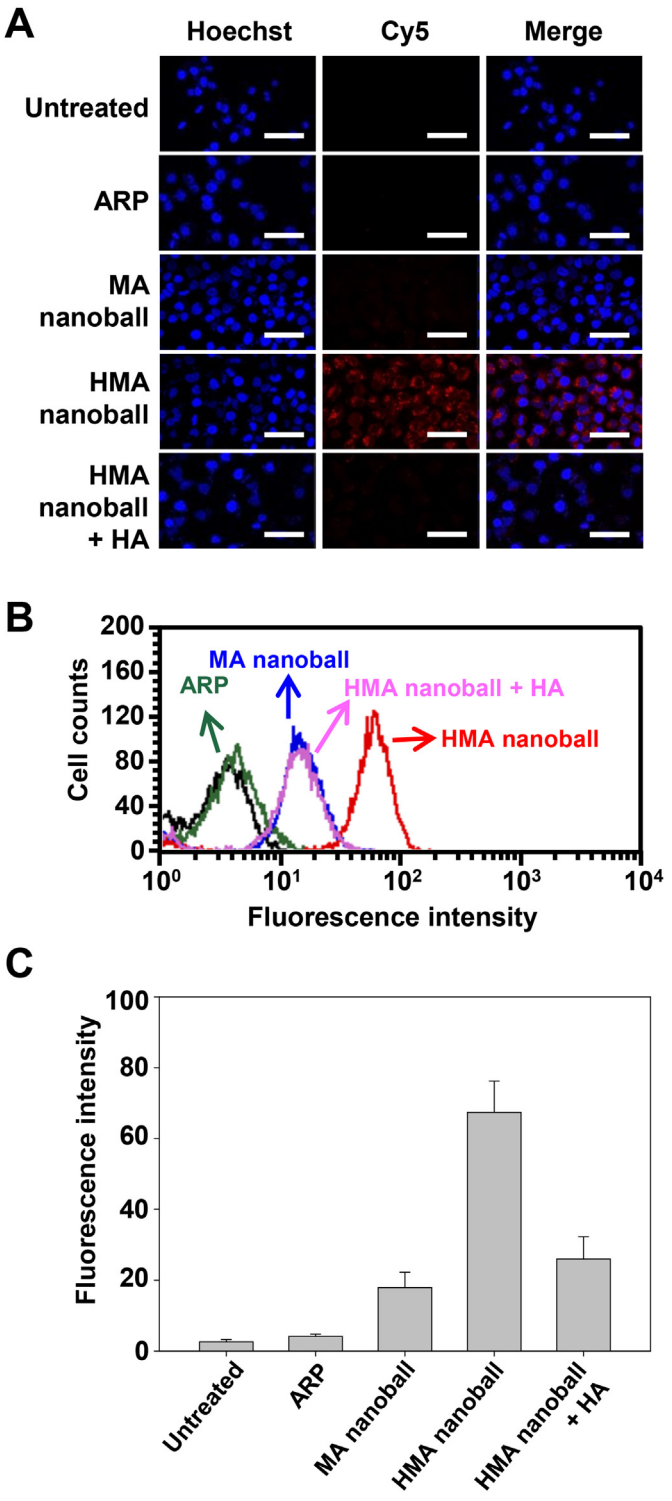

Fig. 3. Cellular uptake of DNA nanoballs. KB cells were left untreated or were treated with ARP, MA nanoballs or HMA nanoballs, with or without HA pre-treatment. Cellular uptake of Cy5-incorporated fluorescent DNA nanoballs was visualized by confocal microscopy (A) and quantified by flow cytometry (B, C). (B) Representative flow cytometry data. (C) Quantification of populations of fluorescence-positive cells. Data are presented as means ± SE (n = 4). Scale bar: 20 μm.

3.2. Characterization of ASO-hybridized DNA nanoballs

The structures of various DNA nanoballs are illustrated in Fig. 2A. Mu peptide-complexed ARP exhibited nanoball-like

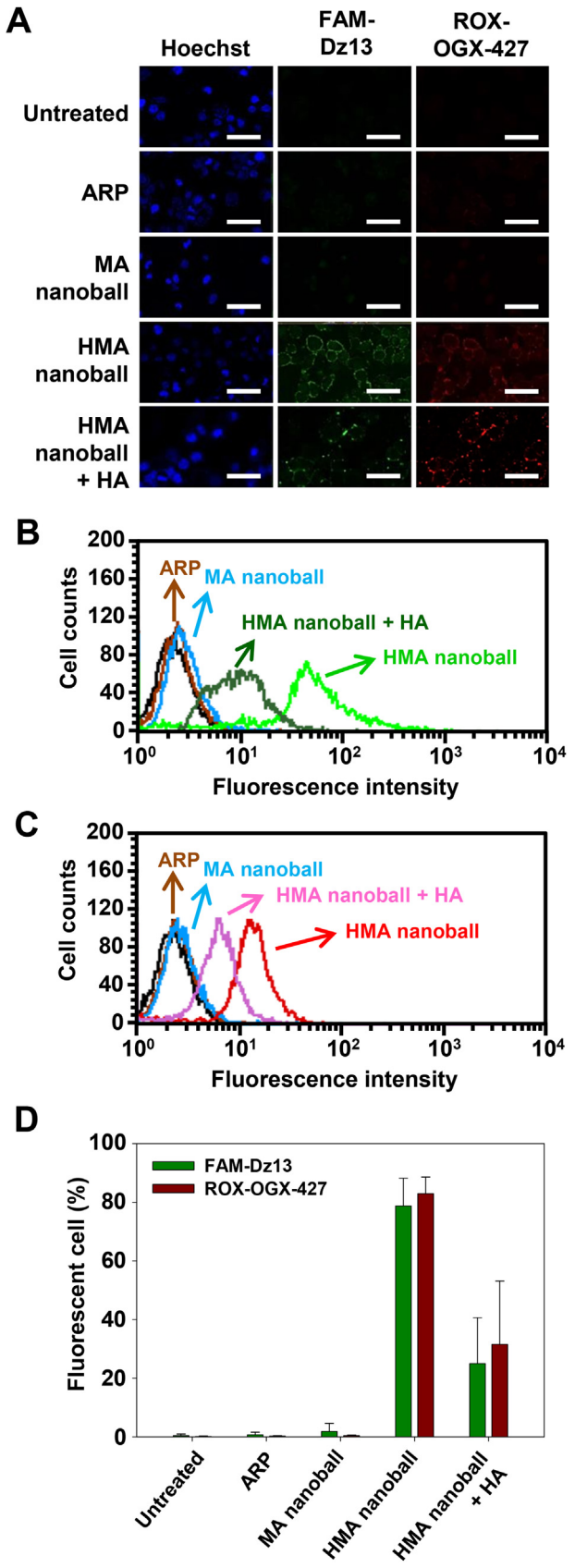

Fig. 4. Cellular uptake of ASOs. KB cells were left untreated or were treated with ARP, MA nanoballs or HMA nanoballs, with or without HA pre-treatment. (A) Cellular uptake of FAM-Dz13 and ROX-OGX-427 ASOs loaded in DNA nanoballs was visualized by confocal microscopy. (B, C) Representative flow cytometry data for cell populations positive for FAM-DZ13 (B) and ROX-OGX427 (C) under various conditions. (D) Flow cytometry-based quantification of populations of fluorescent (ASO-positive) cells. Data are presented as means ± SE (n = 3). Scale bar: 20 μm.

structures (Fig. 2B, C). Surface coating of MA nanoballs with HA retained nanoball-like structures (Fig. 2B, C). The size (Fig. 2D) and zeta potential (Fig. 2E) of ARP were 1242.5 nm ± 320.4 nm and −29.1 mV ± 11.5 mV, respectively. Addition of cationic Mu peptide reduced the size to 162.7 nm ± 32.4 nm and increased the zeta potential to 5.0 mV ± 1.4 mV. After surface coating with HA, the size of nanoballs was 191.4 nm ± 15.1 nm, and the zeta potential was −21.8 mV ± 0.7 mV. Both MA nanoballs and HMA nanoballs showed stability against nucleases (Fig. 2F). Upon 30 min treatment with DNase I, ARP completely degraded and migrated to the bottom of agarose gels. In contrast, agarose gel electrophoresis showed no degraded DNA fragments of MA nanoballs or HMA nanoballs after DNase I treatment. Thus, adenovirus-derived cationic Mu peptide substantially decreased the size of ARP, increased their zeta potential values, and provided stability against nuclease.

3.3. Cellular uptake of DNA nanoballs and dual ASOs

HMA nanoballs entered KB cells via CD44 receptors. To visualize and quantitate the cellular uptake of DNA nanoballs, we used Cy5-incorporated DNA nanoballs by running RCA using Cy5-dCTP. Confocal microscopy (Fig. 3A) and flow cytometry (Fig. 3B, C) showed little uptake of Cy5-dCTP-incoroporated fluorescent ARP or MA nanoballs by CD44-overexpressing KB cells, but revealed considerable entry of fluorescent HMA nanoballs into KB cells. The enhanced cellular uptake of MA nanoballs caused by HA-coating was not observed when the cells were pretreated with free HA.

As a complementary approach, we examined cellular uptake of DNA nanoballs containing hybridized, fluorescently labeled ASOs. Consistent with the above results, confocal microscopy (Fig. 4A) and flow cytometry showed considerable entry of FAM-conjugated DZ13 (Fig. 4B) and ROX-conjugated OGX-427 (Fig. 4C) into CD44-overexpressing KB cells, but little uptake of these fluorescent ASOs when hybridized to MA nanoballs, which lack HA (Fig. 4D). Again, this enhancement of cellular uptake of MA nanoballs by HA-coating was eliminated by pretreating cells with free HA. Collectively, these results confirm the CD44 receptor-dependence of HMA nanoball uptake.

3.4. Reduction of target protein expression by DNA nanoballs

We next investigated the effect of HMA nanoballs on the expression levels of proteins targeted by the dual hybridized ASOs: c-Jun, the target of the DNAzyme Dz-13, and Hsp27, the target of OGX-427. Downregulation of target proteins was monitored by Western blotting (Fig. 5), which showed that treatment of KB cells with HMA nanoballs decreased the protein levels of c-Jun and Hsp27 to 33.0% ± 9.5% (Fig. 5A) and 12.6% ± 7.2% (Fig. 5B) of control levels, respectively. In contrast, treatment of KB cells with HM or MA nanoballs alone did not significantly reduce the levels of either protein (Fig. 5C).

3.5. In vitro anticancer effects of DNA nanoballs

Among the various DNA nanoballs, HMA nanoballs showed the greatest in vitro anticancer effect and synergized with Dox to further enhance anticancer efficacy. CCK-8 assay results reveal that the survival of KB cells was not significantly reduced by treatment with ARP, HM, or MA nanoballs (Fig. 6A). However, treatment of KB cells with HMA nanoballs reduced the survival of KB cells to

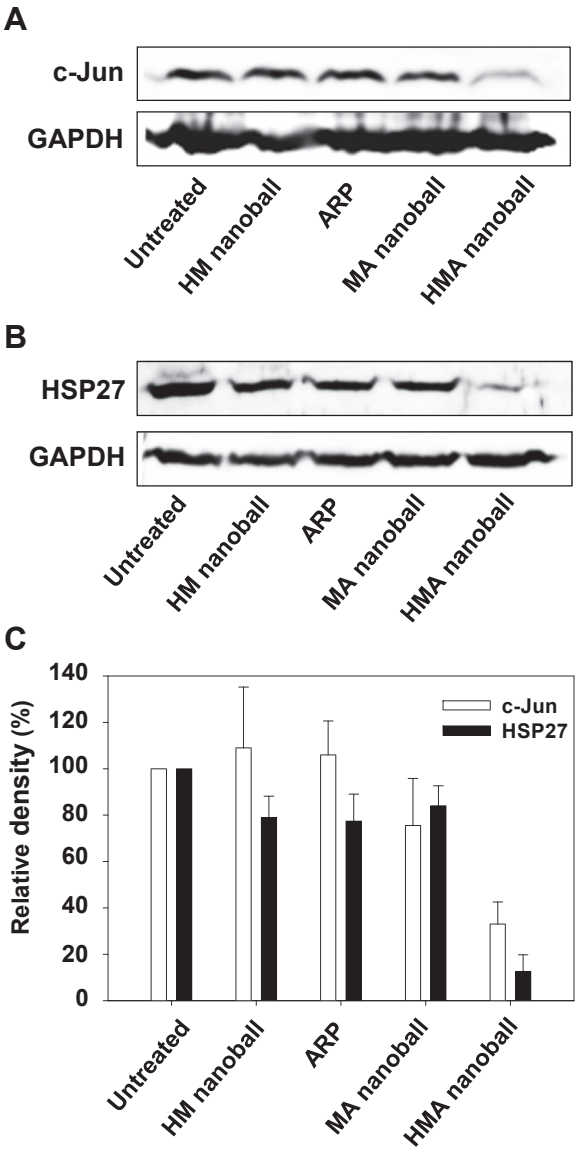

Fig. 5. Reduction of target proteins. The cellular protein levels of target genes, c-Jun (A) and Hsp27 (B), were measured by Western blotting. After various treatments, whole-cell extracts of KB cells were analyzed for target proteins by Western blotting. The data are expressed as means ± SE (n = 3). (C) Relative intensities of c-Jun and Hsp27 normalized to the GAPDH signal.

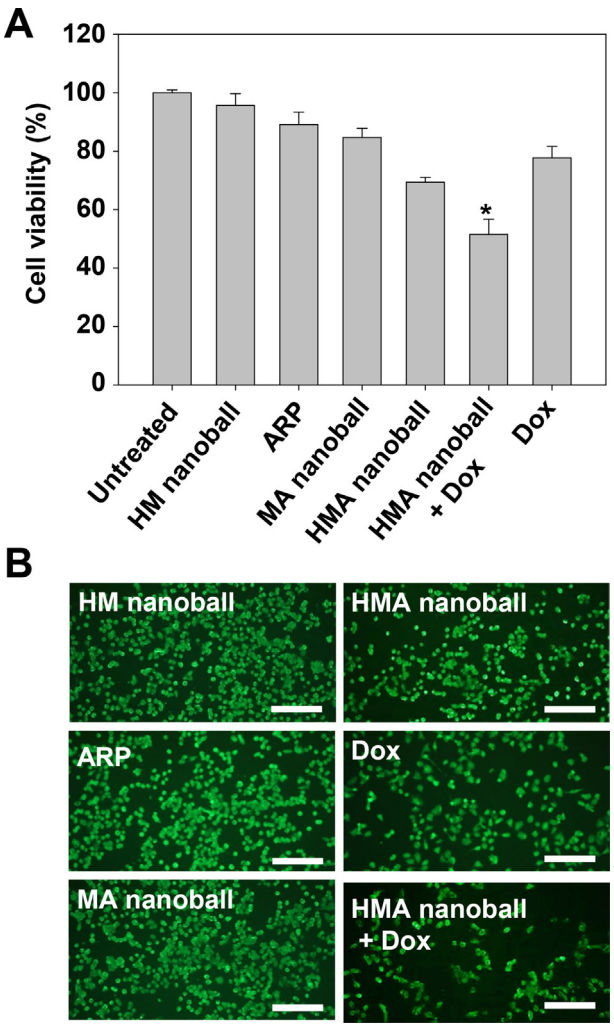

Fig. 6. In vitro tumor cell-killing effect. (A) KB cells were treated with ARP, MA nanoballs, HM nanoballs, or HMA nanoballs in the presence or absence of Dox for 1 h. After media replacement, the cells were incubated for an additional 24 h. The survival of cancer cells was determined by CCK-8 assay. Data are presented as means ± SE (n = 4). *: significantly different from the groups treated with HMA nanoballs or Dox alone (ANOVA and Student–Newman–Keuls test, $p < 0.05$). (B) The live cell population was stained with calcein-AM and observed by fluorescence microscopy. Scale bar: 20 μm.

69.3% ± 1.7% of control levels; co-treatment of KB cells with Dox and HMA nanoballs further reduced survival to 51.5% ± 5.1% (Fig. 6A). Similar to the CCK-8 assay results, the fluorescent microscopy of live cells exhibited the lowest live cell populations in the group treated with HMA nanoballs (Fig. 6B).

3.6. Biodistribution and in vivo anti-tumor effects of DNA nanoballs

We next examined the effect of surface coating with HA on tumor tissue accumulation and anti-tumor effects of intravenously administered MA nanoballs. For molecular imaging, Cy5-incorporated fluorescent nanoballs were injected into KB cell tumor-bearing nude mice. The tumor tissue distribution of Cy5-incorporated HMA nanoballs 1 h post-dose was greater than that of Cy5-incorporated MA nanoballs (Fig. 7A). At 24 h post-injection, total photon counts in tumor tissues were 5.9-fold higher in the HMA nanoball-treated group than in the MA nanoball-treated group (Fig. 7B).

Collectively, these results indicate that surface coating of MA nanoballs with HA enhances tumor tissue accumulation. Systemic co-administration of HMA nanoballs with Dox synergistically inhibited tumor growth in a KB cell xenograft mouse model. Compared to other groups, the HMA nanoball-treated group showed the lowest tumor volume (Fig. 8A) and weight (Fig. 8B).

4. Discussion

Here, we demonstrated that the adenovirus-derived Mu peptide played an essential role in condensing ARP to form MA nanoballs, and surface coating with HA promoted CD44 receptor-mediated delivery of HMA nanoballs to tumor cells. Importantly, ASOs delivered by HMA nanoballs silenced the expression of their target mRNAs of ASO, exerting potent anticancer effects in vitro and in vivo upon co-treatment with Dox.

The goal of this study was to test the delivery of therapeutic oligonucleotides via nucleic acid-based DNA nanoballs using

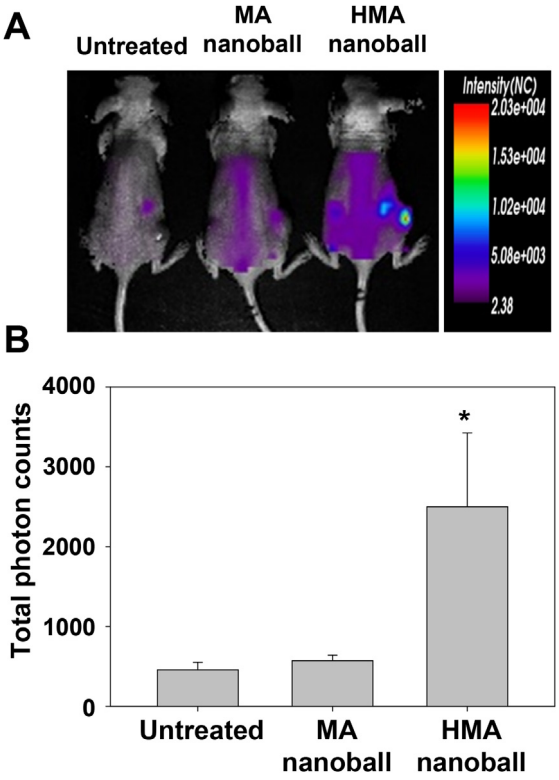

Fig. 7. Biodistribution of ASO-loaded DNA nanoballs. (A) KB tumor-bearing mice were intravenously injected with ARP, MA nanoballs, or HMA nanoballs containing Cy5-dCTP. The biodistribution of Cy5 fluorescence was visualized using a molecular imaging system. (B) The total photon counts of tumor tissues from treated mice were quantified 1 h post-administration by in vivo imaging and compared with those of the untreated group.

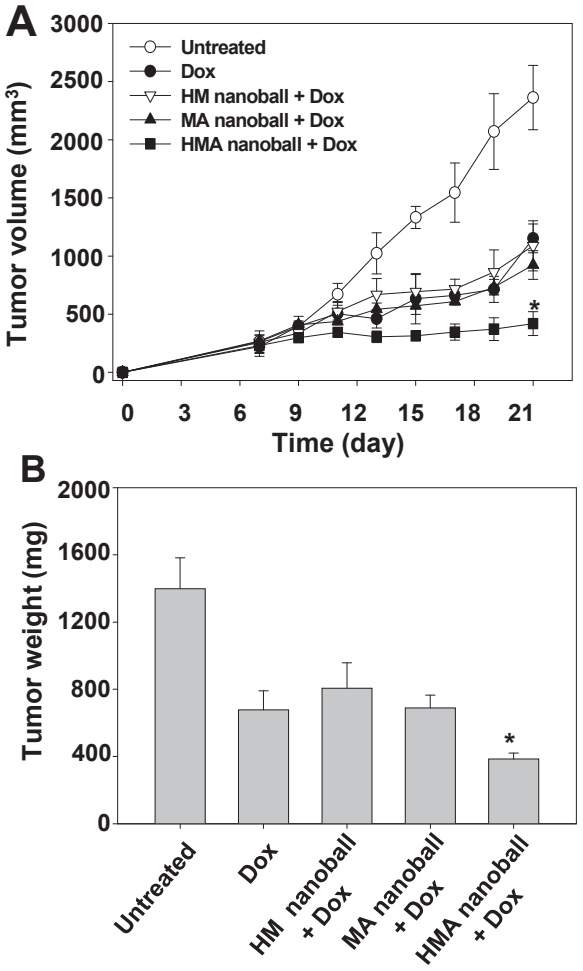

Fig. 8. In vivo anti-tumor effect of ASO-loaded DNA nanoballs. KB tumor-bearing mice were intravenously injected with HM nanoballs, MA nanoballs, or HMA nanoballs (8 mg DNA/kg) and Dox (3 mg Dox/kg) or with Dox alone (3 mg Dox/kg) every other day beginning on day 7 for a total of three injections. For MA and HMA nanoballs, the dose of both ASOs was 2 mg/kg. Tumor sizes were measured until day 21 (A), and tumor tissues were extracted and weighed (B).

sequence-specific hybridization as a loading technique. ssDNA amplified by an RCA reaction can serve as an ASO sequence-specific carrier owing to its thousands of complementary sequences to the ASO. Compared to a scrambled RCA template, RCA templates containing ASO-binding sequences hybridize substantially higher amounts of ASO per RCA product (Fig. 1D). This high hybridization capacity supports the feasibility of using hybridization-mediated ASO loading of RCA products for sequence-specific ASO delivery.

Dual ASOs—Dz13 and OGX-427—were loaded onto HMA nanoballs in a sequence-specific manner (Fig. 1B). Dz13 is a DNAzyme with RNA-binding hybridization arms that cleaves the mRNA of c-Jun, which is involved in cellular proliferation, transformation, and cell death [13]. OGX-427 is known to inhibit the expression of Hsp27, which is involved in cancer progression and cell death [14]. Overexpression of the targets of the two ASOs, c-Jun [15,16] and Hsp27 [17], has been reported in cancer cells.

The adenovirus core complex-derived Mu peptide was used for biomimetic condensation of micrometer-to nanometer-sized DNA balls (Fig. 2). In the absence of Mu peptide, the dual ASO-loaded ssDNAs tended to form a soft, "ball" in solution with a diameter of approximately 1.2 μm (Fig. 2D). Our observations are consistent with a previous report, which showed that micrometer-sized DNA balls are produced by an RCA reaction [18,19]. The interaction between ARP and cationic Mu peptides is electrostatic, resulting in an increase in the zeta potential after condensation (Fig. 2E). Mu peptides have previously been used to condense plasmid DNA and to facilitate plasmid DNA delivery [20,21].

We observed that uptake of ASO by CD44 receptor-overexpressing KB cells was enhanced by delivery using HMA nanoballs compared with MA nanoballs (Figs. 3 and 4), supporting the role of the HA moiety in enhancing CD44 receptor-mediated cellular delivery of DNA nanoballs. HA has been previously reported to increase the tumor cell delivery of nanoparticles by interacting with CD44 receptors; when conjugated to ASOs, it enhances their cellular delivery [22]. Moreover, surface coating of graphene nanosheets with HA has been shown to enhance cellular delivery through CD44 receptors [23], and HA-coated nanocarriers have been designed for delivery of anticancer drug to tumors expressing CD44 receptors [24].

The reduction in target protein levels after treatment of cells with HMA nanoballs is attributable to the enhanced uptake of nanoballs via the HA moiety and implies effective delivery of ASOs to the interior of the cell. The reduced cellular uptake of HMA nanoballs (Fig. 3) and ASO (Fig. 4) after pre-treatment with HA supports the conclusion that the entry of HMA nanoballs into KB cells is mediated by the CD44 receptor. Although further study will be required to elucidate the intracellular fate of HMA nanoballs, we speculate that HMA nanoballs may be partially degraded in endolysosomes, enabling escape of ASOs into the cytosol and binding to target mRNA.

Owing to the greater affinity of the ASOs, Dz13 and OGX-427, for

their target mRNA compared to that for the complementary ASO-binding sequence, the uptake of HMA nanoballs into cells resulted in the dissociation of ASOs from HMA nanoballs and binding to their target mRNA. In addition to the natural preference of ASOs for their natural target mRNAs, dissociation of ASOs from ARP was further facilitated by modifying the RCA template for complementary binding with ASO to contain one mismatched base pair for each ASO. Such facilitated dissociation caused by a single mismatch has been previously demonstrated [25].

We observed the greatest in vivo anti-tumor effect following combined treatment with Dox and HMA nanoballs (Fig. 8). The target proteins of two ASOs, Dz13 and OGX-427, have been reported to be involved in the anticancer mechanisms by Dox [26,27]. Treatment of small lung cancer cells with Dox was shown to induce multidrug resistance protein 1 [26]. In the study, the inhibition of c-Jun phosphorylation was observed to reduce the Dox-induced multidrug resistance protein 1 expression and increase sensitivity of the small lung cancer cells to Dox [26]. Overexpression of Hsp27, the target protein of OGX-427, was found to decrease the intracellular level of topoisomerase II, which is important for sensitivity and initiation of apoptosis by Dox [27]. Specific inhibitors of c-Jun and Hsp27 were found to increase chemosensitivity of cancer cells to Dox [28,29]. Inhibition of c-Jun by Dz13 was shown to enhance the sensitivity of cancer cells to Dox treatment [28]. A recent study reported that the reduced expression of Hsp27 by resveratrol or short hairpin interfering RNA could sensitize MCF-7 breast cancer cells to Dox [29]. Based on these findings, the higher in vivo anti-tumor activity of HMA nanoballs with co-treatment of Dox would be in part due to the enhanced chemosensitivity of KB cells to Dox by reduction of c-Jun and Hsp27.

Moreover, the enhanced in vivo anti-tumor activity in the Dox/HMA nanoball co-treatment group could be attributable to the higher tumor accumulation of HMA revealed by molecular imaging (Fig. 7). The improved stability of HMA nanoballs against DNase I could contribute to prolonging the circulation of DNA nanoballs in serum following intravenous administration. Our in vitro fluorescence microscopy and flow cytometry data revealed that the cellular uptake of HMA nanoballs and ASO significantly reduced after pre-treatment with free HA, supporting the possibility of enhanced tumor distribution of CD44-positive KB xenografted mice. In addition to the free HA pre-treatment, the comparison of cellular uptake by CD44-negative non-cancer cells and CD44-positive cancer cells needs to be done for supporting CD44-mediated uptake of HMA nanoballs in the future. Previously, to test whether HA microparticles enter tumor cells by CD44 receptor-mediated endocytosis in vivo, the tumor accumulation patterns of HA microparticles were compared between CD44-positive and CD44-negative tumor-bearing mice [30]. Since MA nanoballs and HMA nanoballs differ in the surface charges, we can't exclude the contribution of negative surface charges of HMA nanoballs to the in vivo tumor distribution. It would be necessary to compare the distribution and anti-tumor activity of HMA nanoballs in CD44-positive and CD44-negative tumor-xenografted mice models.

5. Conclusions

In this study, biomimetic HMA nanoballs were developed for in vitro and in vivo delivery of functional oligonucleotides. RCA was used to amplify ASO-binding sequences, and dual ASOs were loaded onto HMA nanoballs through sequence-specific complementary hybridization. Soft, ball-shaped, ASO-loaded RCA products were condensed to nanoballs upon biomimetic condensation with adenovirus core complex-derived Mu peptide. Surface coating of MA nanoballs with HA facilitated the delivery of ASOs to cells and reduced the levels of target mRNAs. Co-treatment of HMA nanoballs with Dox improved anti-tumor efficacy. Although we used OGX-427 and Dz13 as model ASOs, the application of HMA nanoballs as an ASO delivery nanoplatform could be extended by replacing the ASO-binding sequences of the RCA template and hybridizing with other therapeutic ASOs. Our results thus suggest the potential of HMA nanoballs for non-cationic and sequence-specific oligonucleotide delivery systems.

Acknowledgment

This work was supported by research grants from the Ministry of Science, ICT and Future Planning (NRF-2014K2A2A4001156, NRF-2015R1A2A1A01005674), and from the Ministry of Trade, Industry & Energy (Technology Innovation Program, Grant No. 10050648), Republic of Korea.

References

[1] R. Kole, A.R. Krainer, S. Altman, RNA therapeutics: beyond RNA interference and antisense oligonucleotides, Nat. Rev. Drug Discov. 11 (2012) 125–140.
[2] H. Cai, F.S. Santiago, L. Prado-Lourenco, B. Wang, M. Patrikakis, M.P. Davenport, et al., DNAzyme targeting c-jun suppresses skin cancer growth, Sci. Transl. Med. 4 (2012) 1–12.
[3] D. Luvino, S. Khiati, K. Oumzil, P. Rocchi, M. Camplo, P. Barthélémy, Efficient delivery of therapeutic small nucleic acids to prostate cancer cells using ketal nucleoside lipid nanoparticles, J. Control Release 172 (2013) 954–961.
[4] B.A. Hadaschik, J. Jackson, L. Fazli, A. Zoubeidi, H.M. Burt, M.E. Gleave, et al., Intravesically administered antisense oligonucleotides targeting heat-shock protein-27 inhibit the growth of non-muscle-invasive bladder cancer, BJU Int. 102 (2008) 610–616.
[5] M.L. Tan, D.E. Dunstan, A.M. Friedhuber, P.F. Choong, C.R. Dass, A nanoparticulate system that enhances the efficacy of the tumoricide Dz13 when administered proximal to the lesion site, J. Control Release 144 (2010) 196–202.
[6] B. Ballarín-González, K.A. Howard, Polycation-based nanoparticle delivery of RNAi therapeutics: adverse effects and solutions, Adv. Drug Deliv. Rev. 64 (2012) 1717–1729.
[7] W. Zhao, C.H. Cui, S. Bose, D. Guo, C. Shen, W.P. Wong, Bioinspired multivalent DNA network for capture and release of cells, Proc. Natl. Acad. Sci. U. S. A 109 (2012) 19626–19631.
[8] G.D. Hamblin, K.M. Carneiro, J.F. Fakhoury, K.E. Bujold, H.F. Sleiman, Rolling circle amplification-templated DNA nanotubes show increased stability and cell penetration ability, J. Am. Chem. Soc. 134 (2012) 2888–2891.
[9] J.B. Lee, S. Peng, D. Yang, Y.H. Roh, H. Funabashi, N. Park, et al., A mechanical A mechanical metamaterial made from a DNA hydrogel, Nat. Nanotechnol. 7 (2012) 816–820.
[10] J.B. Lee, J. Hong, D.K. Bonner, Z. Poon, P.T. Hammond, Self-assembled RNA interference microsponges for efficient siRNA delivery, Nat. Mater. 11 (2012) 316–322.
[11] Z. Zhang, M.M. Ali, M.A. Eckert, D.K. Kang, Y.Y. Chen, L.S. Sender, A polyvalent aptamer system for targeted drug delivery, Biomaterials 34 (2013) 9728–9735.
[12] M. Zöller, CD44: can a cancer-initiating cell profit from an abundantly expressed molecule? Nat Rev Cancer 11 (2011) 254–267.
[13] M. Elahy, C.R. Dass, Dz13: c-Jun downregulation and tumour cell death, Chem. Biol. Drug Des. 78 (2011) 909–912.
[14] V. Baylot, C. Andrieu, M. Katsogiannou, D. Taieb, S. Garcia, S. Giusiano, et al., OGX-427 inhibits tumor progression and enhances gemcitabine chemotherapy in pancreatic cancer, Cell Death Dis. 2 (2011) e221.
[15] E. Park, H. Kang, J. Kim, J. Ko, The role of sLZIP in transcriptional regulation of c-Jun and involvement in migration and invasion of cervical cancer cells, Cell Physiol. Biochem. 33 (2014) 151–164.
[16] C.C. Huang, J.M. Wang, U. Kikkawa, H. Mukai, M.R. Shen, I. Morita, et al., Calcineurin-mediated dephosphorylation of c-Jun Ser-243 is required for c-Jun protein stability and cell transformation, Oncogene 27 (2008) 2422–2429.
[17] C. Dobo, J.N. Stavale, O. Lima Fde, D.A. Ribeiro, V. Arias, T.S. Gomes, et al., HSP27 is commonly expressed in cervical intraepithelial lesions of Brazilian women, Asian Pac. J. Cancer Prev. 14 (2013) 5007–5010.
[18] J. Jarvius, J. Melin, J. Göransson, J. Stenberg, S. Fredriksson, C. Gonzalez-Rey, et al., M.Digital quantification using amplified single molecule detection, Nat. Methods 3 (2006) 725–727.
[19] S. Huang, Y. Chen, Polymeric sequence probe for single DNA detection, Anal. Chem. 83 (2011) 7250–7254.
[20] R. Rajagopalan, J. Xavier, N. Rangaraj, N.M. Rao, V. Gopal, Recombinant fusion proteins TAT-Mu, Mu and Mu-Mu mediate efficient non-viral gene delivery, J. Gene Med. 9 (2007) 275–286.
[21] P. Saccardo, A. Villaverde, N. Gonzalez-Montalban, Peptide-mediated DNA condensation for non-viral gene therapy, Biotechnol. Adv. 27 (2009) 432–438.
[22] H. Mok, J.W. Park, T.G. Park, Antisense oligodeoxynucleotide-conjugated

hyaluronic acid/protamine nanocomplexes for intracellular gene inhibition, Bioconjug. Chem. 18 (2007) 1483–1489.
[23] W. Miao, G. Shim, C.M. Kang, S. Lee, Y.S. Choe, H.G. Choi, et al., Cholesteryl hyaluronic acid-coated, reduced graphene oxide nanosheets for anti-cancer drug delivery, Biomaterials 34 (2013) 9638–9647.
[24] R. Mo, T. Jiang, R. DiSanto, W. Tai, Z. Gu, ATP-triggered anticancer drug delivery, Nat. Commun. 5 (2014) 1–10.
[25] L. Yao, Y. Wang, S. Xu, Label-free microRNA detection based on exchange-induced remnant magnetization, Chem. Commun. 49 (2013) 5183–5185.
[26] C. Shinoda, M. Maruyama, T. Fujishita, J. Dohkan, H. Oda, K. Shinoda, et al., Doxorubicin induces expression of multidrug resistance-associated protein 1 in human small cell lung cancer cell lines by the c-jun N-terminal kinase pathway, Int. J. Cancer 117 (2005) 21–31.
[27] R.K. Hansen, I. Parra, P. Lemieux, S. Oesterreich, S.G. Hilsenbeck, S.A. Fuqua, Hsp27 overexpression inhibits doxorubicin-induced apoptosis in human breast cancer cells, Breast Cancer Res. Treat. 56 (1999) 187–196.
[28] C.R. Dass, L.M. Khachigian, P.F. Choong, c-Jun knockdown sensitizes osteosarcoma to doxorubicin, Mol. Cancer Ther. 7 (2008) 1909–1912.
[29] J. Díaz-Chávez, M.A. Fonseca-Sánchez, E. Arechaga-Ocampo, A. Flores-Pérez, Y. Palacios-Rodríguez, G. Domínguez-Gómez, et al., Proteomic profiling reveals that resveratrol inhibits HSP27 expression and sensitizes breast cancer cells to doxorubicin therapy, PLoS One 8 (2013) e64378.
[30] S.-D. Li, S.B. Howell, CD44-targeted microparticles for delivery of cisplatin to peritoneal metastases, Mol. Pharm. 7 (2010) 280–290.